Journal of Immunology and Regenerative Medicine 19 (2023) 100070

Contents lists available at ScienceDirect

Journal of Immunology and Regenerative Medicine

journal homepage: www.elsevier.com/locate/regen

Calcium phosphate with submicron topography influences primary human macrophage response, enhancing downstream angiogenesis and osteogenesis *in vitro*

L.A. van Dijk [a,b,d], L. Utomo [a,c], H. Yuan [b], F. Barrère-de Groot [b], D. Gawlitta [a,d], A.J.W.P. Rosenberg [a], J.D. de Bruijn [b,e,*]

[a] Department of Oral and Maxillofacial Surgery and Special Dental Care, University Medical Center Utrecht, Utrecht University, the Netherlands
[b] Kuros Biosciences BV, Bilthoven, the Netherlands
[c] Department of Clinical Sciences, Faculty of Veterinary Medicine, Utrecht University, Utrecht, the Netherlands
[d] Regenerative Medicine Center Utrecht, Utrecht, the Netherlands
[e] Queen Mary University of London, UK

ARTICLE INFO

Keywords:
Calcium phosphate
Bone graft substitutes
Surface topography
Macrophages
Osteoimmunology

ABSTRACT

Calcium phosphates with submicron surface features have demonstrated superior performance to conventional calcium phosphates and equivalence to autologous bone in pre-clinical bone healing models. This is related to their ability to form bone in soft tissues, without the addition of cells and growth factors. It is hypothesized that a specific innate immune response to submicron topography contributes to the enhanced bone healing by these materials. Upregulation of pro-healing, anti-inflammatory 'M2' macrophages versus pro-inflammatory 'M1' macrophages on submicron-structured calcium phosphates may be involved. In this *in vitro* study, the response of primary human macrophages to different calcium phosphate bone graft substitutes was assessed. Primary $CD14^+$ monocytes were isolated from human buffy coats and were seeded on two different calcium phosphate materials. The first material had a submicron topography of needle-shaped crystals ($BCP_{<\mu m}$) while the second material had no submicron topography (TCP). Macrophage M1/M2 phenotype characterization by protein and gene expression markers at 24 h and 72 h indicated overall stronger macrophage activation and subtle phenotypic skewing towards the M2 phenotype on $BCP_{<\mu m}$ vs TCP. Moreover, macrophages exhibited an elongated morphology on $BCP_{<\mu m}$, which is associated with the M2 phenotype, while macrophages on TCP primarily exhibited a spherical morphology. Conditioned medium of macrophages cultured on $BCP_{<\mu m}$ resulted in enhanced *in vitro* angiogenic tube formation and osteogenic differentiation of mesenchymal stromal cells, compared to conditioned medium from macrophages on TCP. Altogether, these findings suggest a potential role of M2 macrophage upregulation in the bone-induction mechanism of calcium phosphates with submicron surface topography.

1. Introduction

Calcium phosphate ceramics are among the most well-studied synthetic bone graft substitute materials, due to their excellent biocompatibility, osteoconductive, and bioactive properties.[1] The efficacy of calcium phosphate bone graft materials has been correlated with specific physicochemical properties, including phase composition,[2–4] micro- and macroporosity,[5–7] and surface features.[8–10] Ongoing developments in material engineering, specifically the modification of surface features, have resulted in calcium phosphate bone graft materials that demonstrate improved efficacy compared to conventional calcium phosphates.[8,10–14] Surface features in the submicron scale, *i.e.* pores and crystals <1 μm in dimension, have been demonstrated to be associated with osteoinductive potential of calcium phosphates (*i.e.* capacity to induce *de novo* bone formation). These materials also exhibit an ability to repair critical-sized bone defects that approaches the efficacy of the 'gold standard' bone autograft, without addition of exogenous cells and/or growth factors.[8–10,12,14–16] The relationship between surface features and bone-inducing potential of calcium phosphates has so far been demonstrated in various animal models, including mouse, rabbit, goat, sheep, canine and baboon.[17] Recently, we have demonstrated accelerated bone formation in soft tissue by calcium phosphate

* Corresponding author. Professor Bronkhorstlaan 10, Building 48, 3723 MB, Bilthoven, the Netherlands.
E-mail address: j.d.debruijn@qmul.ac.uk (J.D. de Bruijn).

https://doi.org/10.1016/j.regen.2023.100070
Received 31 October 2022; Received in revised form 23 December 2022; Accepted 22 January 2023
Available online 23 January 2023

with a topography of submicron needle-shaped crystals compared to calcium phosphate with submicron grain-shaped crystals.[9] This material also exhibited equivalence to autograft and superiority to conventional ceramics in challenging spinal fusion models.[12,15,18]

To understand the mechanisms behind the enhanced healing response to submicron surface structured calcium phosphates, it is helpful to consider the biological events that occur after implantation that ultimately lead to bone formation. In the early phases after implantation (hours-days), before interaction of osteogenic cells with the material, initial tissue responses are mostly dictated by cells of the innate immune system.[19,20] A healthy immune response is a prerequisite for the normal healing of tissue injury.[21] Likewise, a favorable innate immune response to a biomaterial is paramount for successful healing and integration after implantation.[22,23]

Biomaterial implantation is typically followed by a rapid but short-lived invasion of neutrophils that elicit an acute inflammatory response. Hereafter, circulating monocytes are recruited to the implantation site, become activated, and differentiate into macrophages.[20,21] Macrophages are known to play a central role in the innate immune response to tissue injury and biomaterials. They are the key regulators of the wound healing process, in which they evolve to adopt distinct phenotypes during the different stages of healing.[24] Macrophage phenotypes are broadly categorized into those having a pro-inflammatory role, better known as the 'classically' activated or 'M1' phenotype, and on the other hand macrophages with an anti-inflammatory function, commonly described as the 'alternatively' activated, 'M2' or 'pro-healing' phenotype.[25,26] M1 macrophages promote inflammation by release of pro-inflammatory cytokines and produce harmful reactive oxygen species to clear pathogens, debris, and foreign materials. M2 macrophages aim to resolve inflammation by secretion of anti-inflammatory factors and facilitate tissue repair and remodeling by signaling to local progenitor cells and stem cells responsible for tissue regeneration.[24,27] Transition between M1 and M2 phenotypes can occur swiftly in response to environmental stimuli, such as cytokines, pathogens, and materials.[21,24,26–28]

During the normal healing cascade, the macrophage population is dominated by M1 macrophages during the acute inflammatory phase and will then gradually shift towards an M2-dominated population to create the pro-healing environment required for regeneration.[24,28] However, when the transition to M2 macrophages is inhibited, for example due to a bioincompatible implant, the prolonged presence of inflammatory M1 macrophages can exacerbate tissue injury and prevent biomaterial integration.[28–30] The associated chronic inflammatory state can lead to undesirable outcomes, such as granuloma formation, fibrosis and ultimately fibrous encapsulation of the implant, known as the foreign body response.[20,22,29,31]

Research in the field of osteoimmunology has established that there exists an intricate relationship between macrophages, and bone tissue formation and homeostasis.[29,32,33] M2-like tissue-resident osteal macrophages, termed OsteoMacs, have been shown to directly regulate osteoblast survival and bone matrix deposition *in vivo*.[34,35] Macrophages have displayed intricate crosstalk with mesenchymal stem cells (MSCs) that leads to osteogenic differentiation.[36,37] Recently, Zhang et al. reported a correlation between accelerated fracture healing and greater percentages of M2 macrophages in fracture calluses in human patients.[38] In contrast, upregulated M1 macrophage populations have been associated with destructive bone resorption in bisphosphonate-related osteonecrosis of the jaw.[39–41] Strategies to augment M2 macrophage activation during bone defect repair have demonstrated enhanced bone formation and implant osseointegration associated with greater numbers of M2 macrophages.[42–47] Recently, an M2 macrophage-like cell population has been recognized to have an important role in the process of heterotopic ossification, which is similar to material-induced ectopic bone formation.[48,49]

In this context, the macrophage response is deemed highly relevant in bone regeneration utilizing calcium phosphate bone graft substitute materials.[33] Previously, local depletion of monocytes/macrophages has been shown to block *in vivo* ectopic bone formation by calcium phosphate with submicron surface features.[50,51] Moreover, recent results have indicated murine M2 macrophage upregulation by calcium phosphate materials with osteoinductive capacity.[51,52]

In the current study, we set out to assess the *in vitro* response of primary human macrophages to different calcium phosphate bone graft materials. The first material was a biphasic calcium phosphate with a submicron surface topography of needle-shaped crystals ($BCP_{<\mu m}$), which exhibits the ability to form bone in soft tissues without added cells or growth factors, and has demonstrated enhanced bone healing compared to conventional ceramics *in vivo*.[9,12] This material was compared to a conventional tricalcium phosphate that had no submicron topography (TCP), was not osteoinductive[53] and has shown low bone healing potential *in vivo*.[11,12,54,55] The goal of this study was to elucidate whether $BCP_{<\mu m}$ with submicron topography induced stronger M2 macrophage activation than the conventional bone graft material TCP. This would suggest a role of pro-healing M2 macrophages in the enhanced bone healing observed with submicron structured calcium phosphates. Additionally, paracrine effects of macrophages on *in vitro* angiogenic tube formation and osteogenic differentiation of mesenchymal stromal cells were assessed using conditioned medium assays.

2. Materials and methods

2.1. Materials

Two calcium phosphate bone graft materials were used for the experiments. The first material, a biphasic calcium phosphate (±30% HA/70% β-TCP) with a submicron topography of needle-shaped crystals ($BCP_{<\mu m}$, MagnetOs Granules™, Kuros Biosciences B·V., Bilthoven, NL) was manufactured by Kuros Biosciences as described previously.[9,18] In brief, porous BCP blocks were produced from calcium orthophosphate powder using foaming agent and porogen, followed by sintering at 1125 °C for 6 h. The blocks were crushed and sieved to obtain granules of 1–2 mm. The topography of submicron needle-shaped crystals was obtained by autoclaving the granules at 135 °C for 100 min. The second material was purchased as a porous tricalcium phosphate (≥98%–100% β-TCP) with a granule size of 1–2 mm, manufactured by Orthovita Inc. (TCP, Vitoss Morsels, Orthovita Inc., Malvern, PA, USA). The materials were characterized by mercury intrusion porosimetry and measurement of surface crystal size by scanning electron microscopy (SEM, JEOL JSM-5600, JEOL, Akishima, Tokyo, Japan). Both materials were distributed into 400 μl aliquots and were then subjected to dry heat sterilization (3 h at 200 °C). The material properties of $BCP_{<\mu m}$ and TCP are presented in Table 1.

2.2. Monocyte isolation and seeding on biomaterials

Monocytes were isolated from a total of 5 buffy coats (male donors, 42.8 ± 14.9 years) acquired from the local blood bank (Sanquin, Amsterdam, the Netherlands). Primary $CD14^+$ monocytes were obtained through density gradient separation using Ficoll Paque Plus (GE Healthcare Life Sciences, Chicago, USA) and subsequent magnetic activated cell sorting (MACS) using human CD14 microbeads (Miltenyi Biotec, Bergisch Gladbach, Germany), as described previously.[56] Per sample, 400 μl/well of $BCP_{<\mu m}$ or TCP granules were transferred to well plates. The materials were pre-incubated for 2 h at 37 °C in basic culture medium: Roswell Park Memorial Institute (RPMI) 1640 medium with 2.05 mM L-Glutamine (, Gibco, Carlsbad, USA), supplemented with 10% heat-inactivated fetal bovine serum (Biowest) and 100 U/mL penicillin with 100 mg/ml streptomycin (Invitrogen, Carlsbad, USA). Subsequently, $CD14^+$ monocytes were seeded on the calcium phosphate granules at a density of 4.5×10^5 cells/well in 1 ml of basic culture medium supplemented with 10 ng/ml macrophage colony-stimulating factor (M-CSF; Peprotech, New Jersey, USA). The cells were cultured

Table 1
Properties of calcium phosphate materials.

Material		$BCP_{<\mu m}$	TCP
Granule size		1–2 mm	1–2 mm
Chemistry		30 HA/70 TCP	100 TCP
Surface crystal structure[a]		Needle	Grain
Surface crystal size [μm][a]		0.65 ± 0.26	1.70 ± 0.69
Total porosity[b]		80%	74%
Macroporosity[b]		69%	54%
Microporosity[b]		11%	20%
Specific surface area by weight[b] [m2 g^{-1}]		2.77	0.36
Specific surface area by volume[b] [m2 ml^{-1}]		1.78	0.30
Ectopic bone formation[c]	*Bone incidence*	8/8 [d]	0/4 [e]
	Bone in available space %	24.5 ± 4.3 [d]	n/a

[a] Data from measurements on scanning microscopy images (5000 ×).
[b] Data from mercury intrusion.
[c] Previously published data in canine intramuscular implantation model, 12 weeks post-implantation.
[d] [9].
[e] [53].

at 37 °C under humidified conditions at 5% carbon dioxide (CO_2) for 24 h or 72 h, with medium refreshment after 48 h. Macrophage phenotype marker profiles were confirmed in macrophages cultured in monolayers. M1 and M2 macrophage phenotypes were induced by culturing in basic culture medium supplemented with 10 ng/ml MSCF and for M1: 100 ng/ml interferon-gamma +100 ng/ml tumor necrosis factor alpha; and for M2: 20 ng/ml interleukin 4, for 72 h. Macrophage polarization profiles were confirmed in macrophages cultured in monolayers (Supplementary Figures 1, 2). A schematic overview of the experimental procedures is shown in Fig. 1.

2.3. Scanning electron microscopy and cell shape quantification

To visualize the material surfaces both before and after macrophage culture, a scanning electron microscope (SEM) was used (JEOL JSM-5600). For cell culture samples (72 h), granules were rinsed in phosphate buffered saline (PBS, Gibco), fixed in 2.5% glutaraldehyde (Sigma) for 1.5 h, and stored in PBS at 4 °C until further processing. The cells were dehydrated using a graded ethanol series followed by air-drying by evaporation of tetramethylsilane (Sigma, St. Louis, USA). Granules were mounted on specimen mounts and were gold sputter-coated (JEOL JFC 1300) prior to visualization by SEM.

Cell shape quantification was performed on at least 20 different SEM images of macrophages of different donors ($n = 3$) by measuring the shortest and longest axis of each cell through the midline using software (AxioVision LE, Carl Zeiss Microscopy, Oberkochen, Germany). An elongation index was calculated for each cell by dividing the length of the long axis by the short axis. Using this elongation index, the percentage of elongated cells was determined, *i.e.* with an elongation index ≥2.

2.4. Gene expression analysis

Expression of mRNA by macrophages cultured on $BCP_{<\mu m}$ or TCP was analyzed for different donors ($n = 3$) in triplicates. The mRNA was isolated using TRIzol reagent (Thermo Fisher), according to the manufacturer's instructions. Quantification of total extracted RNA was determined using a spectrophotometer (DS-11 series, DeNovix Inc., Wilmington, USA) at 260/280 nm. Subsequently, complementary DNA (cDNA) was synthesized using iScript™ cDNA Synthesis Kit (Bio-Rad, Hercules, USA) following the manufacturer's instructions. Quantitative PCR analysis was performed using a Bio-Rad CFX96 Real-Time PCR Detection System using FastStart SYBR Green Master mix (Roche Molecular Systems, Inc., Pleasanton, USA). Expression of cluster of differentiation 206 (*CD206*; Fw: TGGCCGTATGCCGGTCACTGTTA; Rev: ACTTGTGAGGTCACCGCCTTCCT), *CCL18* (Fw: TTGTGAGTTTC-CAAGCCCCA; Rev: GCAGCAGAGCTCTTTGTTGGTA), *CD163* (Fw: GTTGGCCATTTTCGTCGCATT; Rev: CTCTCCTCTTGAGGAAACTGCAA), C–C motif chemokine ligand 2 (*CCL2*, Fw: AATCACCAGCAG-CAAGTGTC; Rev: TCTTCGGAGTTTGGGTTTGCT), *CCL5* (Fw: TGCTGCTTTGCCTACATTGC; Rev: CACACACTTGGCGGTTCTTT), Interleukin 1β (*IL1β*, Fw: AGCTGATGGCCCTAAACAGA; Rev: TGTAGTGGTGGTCGGAGATT) was analyzed, to discriminate between M1 (*CCL2, CCL5, Il1β*) and M2 (*CD206, CCL18, CD163)* macrophage phenotypes.[57–59] Glyceraldehyde-3-phosphate dehydrogenase (*GAPDH,* Fw: ATGGGGAAGGTGAAGGTCG; Rev: TAAAAGCAGCCCTGGTGACC) was selected as housekeeping gene for primary human monocyte-derived macrophages based on previous work.[60] The efficiency of all primers was between 0.9 and 1.1 and relative expression was calculated using the formula: $2^{-\Delta CT}$.

2.5. Cytokine quantification

After 24 h and 72 h of culture, cell culture supernatants of different

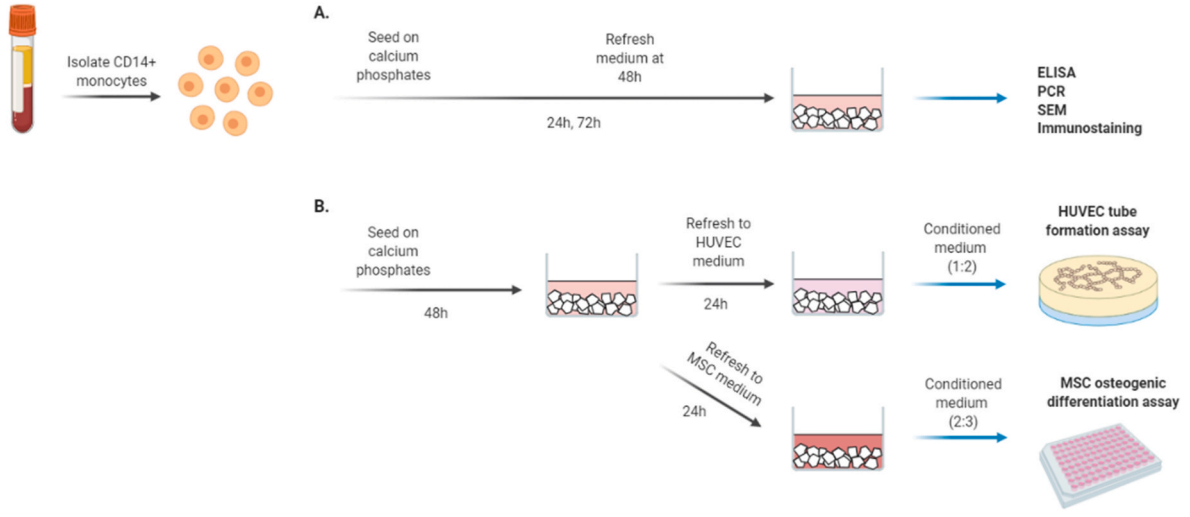

Fig. 1. Schematic overview of the experimental procedures. After isolation, $CD14^+$ monocytes were seeded on $BCP_{<\mu m}$ and TCP to (A) evaluate their response to the materials and (B) to generate macrophage-conditioned medium for use in angiogenic and osteogenic assays.

blood donors ($n = 4$) were collected for cytokine quantification in triplicates by enzyme-linked immunosorbent assays (ELISA). The supernatants were centrifuged for 10 min at 300G, aliquoted, and stored at −80 °C until analysis. Human C–C motif chemokine ligand 18 (CCL18; Duoset ELISA, R&D Systems, Minneapolis, USA), human soluble cluster of differentiation 163 (sCD163; Duoset ELISA, R&D Systems), human C–C motif chemokine ligand 5 (CCL5; Duoset ELISA, R&D Systems), and human interleukin 6 (IL-6; Ready-SET-Go!® ELISA, eBioscience, San Diego, USA) were measured with ELISA kits according to the manufacturers' instructions. Absorbance was measured at 450 nm and corrected at 570 nm (Zenyth 3100 Microplate Multimode Detector, Anthos Labtec Instruments, Salzburg, Austria). These cytokines were selected as indicators of M1 (CCL5, IL-6) and M2 (CCL18, CD163) macrophage phenotype based on literature and were confirmed by induction in monolayers (Appendix Figure A2).[59,61,62] For each sample, measured cytokine concentrations were divided by DNA concentration to normalize.

2.6. DNA quantification

After the removal of supernatant for cytokine quantitation, calcium phosphate granules were rinsed in PBS followed by treatment with PBS/0.1% Triton X-100 (Sigma) for cell lysis. Lysates were collected after 5 min, vortexed and stored at −80 °C until analysis. Quantification of Double stranded DNA was performed using QuantiFluor® dsDNA System (Promega, Madison, USA), according to the manufacturer's instructions. Fluorescence signal was measured with excitation and emission at 504 nm and 531 nm, respectively (Zenyth 3100 Microplate Multimode Detector, Anthos Labtec Instruments).

2.7. Immunofluorescent staining of macrophages

Immunofluorescent staining of macrophages for cluster of differentiation 68 (CD68 (Kp-1), 10 μg/ml, Cell Marque, Rocklin, USA), CD163 (6.7 μg/ml, ab182422, Abcam, Cambridge, UK) and inducible nitric oxide synthase (iNOS, 1:50, ab15323, Abcam) was performed for visualization by confocal microscopy (SP8x, Leica-microsystems, Mannheim, Germany). These antibodies were selected for use as pan-macrophage marker (CD68), M2 phenotype marker (CD163) and M1 phenotype marker (iNOS), based on literature.[63–65] The cells adherent to calcium phosphate granules were fixed in formalin (10%) and stored in PBS at 4 °C until further processing. After permeabilization using PBS/0.2% Triton X-100, non-specific protein binding was blocked using PBS/5% bovine serum albumin (Sigma) prior to incubation with the primary antibody for 1 h. After washing with 0.1% Tween in PBS, cells were incubated for 1 h with a biotinylated secondary antibody (1:200, goat anti-rabbit biotinylated, E0432, Dako; or 1:200, sheep anti-mouse biotinylated, RPN1001v1, GE Healthcare). Next, samples were incubated with tertiary antibody streptavidin Alexa Fluor 568 (5 μg/ml, S11226, Invitrogen) and fluorescein isothiocyanate (FITC)-conjugated Phalloidin (0.5 μg/ml, Sigma) to show the F-actin network. Lastly, cell nuclei were stained with 4',6-diamidino-2-phenylindole dihydrochloride (DAPI, 100 ng/ml) for 10 min. All incubation steps were performed at room temperature under mild agitation. For image capture, Z-stacks were used to obtain a greater depth of field to capture cells in different focal planes on the uneven material surfaces.

2.8. Angiogenic tube formation assay

To evaluate the effect of macrophage conditioned medium (mCM) on angiogenic tube formation, macrophages of different donors ($n = 3$) were cultured in triplicates on $BCP_{<\mu m}$ or TCP for 48 h in basic culture medium, supplemented with 10 ng/ml M-CSF, after which the wells were rinsed in PBS and medium was changed to complete endothelial growth medium-2 (EGM-2, Lonza, Basel, Switzerland), containing Endothelial Basic Medium 2 (EBM-2, Lonza) + Singlequots (Lonza), 5% FBS, 2.05 mM L-Glutamine (Gibco) and 100 U/mL penicillin with 100 mg/ml streptomycin (Invitrogen). After 24 h, mCM was pooled, centrifuged for 10 min at 300G, aliquoted and stored at −80 °C until further use. Human umbilical vein-derived endothelial cells (HUVECs) were expanded to 80% confluence on tissue culture polystyrene coated with 0.1% gelatin. For the tube formation assay, μ-slides for angiogenesis (Ibidi, Gräfelfing, Germany) were coated with growth factor reduced Matrigel (1:1 diluted with PBS, 45 min at 37C°, Corning, New York, USA), after which HUVECs were seeded at a density of 48,000 cells/cm^2 in a 1:1 ratio of mCM and EBM-2 supplemented with 1% FBS, using 6 replicates per condition. As positive and negative control, EBM-2 supplemented with 10% and 0% FBS were used, respectively. Slides were incubated for 16 h at 37 °C under humidified conditions and with 5% CO_2, followed by observation of tube networks and image capture (full-view of wells) by microscopy (IX53, Olympus, Hamburg, Germany). Images were processed for quantification in graphics editor software (Adobe Photoshop CS5, Adobe, San Jose, USA) using fixed parameters for cropping, brightness-contract adjustment and resizing. Tube network images were then quantified using 'Angiogenesis Analyzer for ImageJ'[66] plugin for ImageJ (NIH, Bethesda, USA).

2.9. Osteogenic differentiation of MSCs

To assess the indirect effect of macrophages activated by the materials on the osteogenic differentiation of bone marrow-derived MSCs (BMSCs), conditioned medium from the macrophages (mCM) was prepared. Briefly, macrophages of different blood donors ($n = 3$) were cultured in triplicates on $BCP_{<\mu m}$ or TCP for 48 h in basic culture medium supplemented with 10 ng/ml M-CSF, after which the wells were rinsed in PBS and medium was changed to basic MSC medium: alpha Minimum Essential Medium (αMEM, 22561, Gibco) supplemented with 10% HI-FBS, 100 U/mL penicillin, 100 mg/ml streptomycin (15140, Invitrogen), and 0.2 mM L-ascorbic acid-2-phosphate (ASAP, Sigma). After 24 h, mCMs from multiple wells were pooled, centrifuged for 10 min at 300G, aliquoted, and stored at −80 °C until further use. Human BMSCs were isolated and characterized as previously described.[67] For osteogenic differentiation, BMSCs of one donor were seeded in polystyrene well plates at a density of 3000 cells/cm^2 in basic MSC medium supplemented with 1 ng/ml basic fibroblast growth factor (rh-FGF-2; R&D Systems). After 3 days, medium was refreshed to a 2:3 ratio of, respectively, mCM and osteogenic differentiation medium, containing basic MSC medium supplemented with β-glycerophosphate (BGP, Sigma) to obtain a final concentration of 10 mM BGP. As control conditions, osteogenic differentiation medium and basic culture medium were used. The cells were cultured for 10 days at 37 °C under humidified conditions and 5% CO_2, with media refreshment every 3 days. After 10 days of culture, MSCs were rinsed in PBS and then lysed using PBS/0.2% Triton X-100, prior to storage at −80 °C until further use. Additional samples of each condition were fixed using 10% formalin for later osteonectin immunofluorescence staining.

2.9.1. Quantification of Alkaline Phosphatase activity

Quantification of Alkaline Phosphatase (ALP) activity in MSC lysates was performed as previously described.[68] ALP is a relevant marker of osteogenic differentiation.[69] ALP activity was measured after 10 days based on previous work and reports in literature that ALP levels peak after 10–14 days of osteogenic differentiation.[70] ALP activity in cell lysates was measured by conversion of p-nitrophenyl phosphate (pNPP), using the pNPP liquid substrate system (Sigma) according to the manufacturer's instructions. Absorbance was measured at 405 nm and corrected at 655 nm (Bio-Rad, Hercules, CA). A reference curve of serially diluted known activity of calf intestinal ALP (Sigma) in PBS/0.2% Triton X-100 was used to determine ALP activity in lysates. In addition, DNA content in MSC lysates was used for normalization and was quantified as described above, using QuantiFluor® dsDNA System (Promega, Madison, USA).

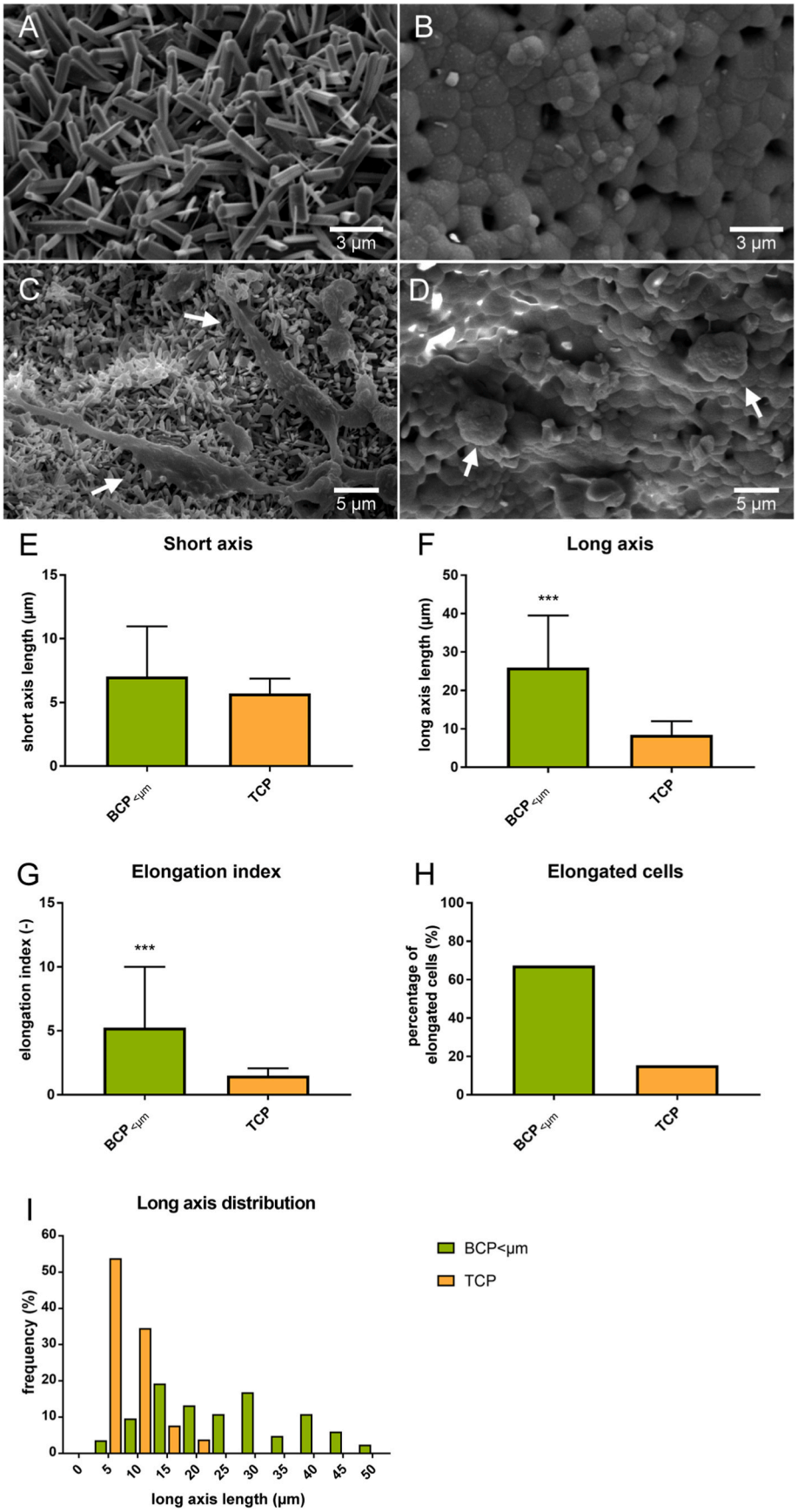

Fig. 2. Cell shape of macrophages cultured on calcium phosphates. SEM images of the surface of (A) $BCP_{<\mu m}$ and (B) TCP, prior to macrophage seeding. SEM image of macrophages (white arrows) adhering to the surface of (C) $BCP_{<\mu m}$ and (D) TCP after 72 h culture. (E, F) Quantification of cell shape analysis of macrophages adherent on $BCP_{<\mu m}$ and TCP. The length of the short axis and long axis of macrophages was measured on a total of 53 images (20 TCP, 33 BCP), with on average two cells per image. (G, H) Short axis and long axis length were used to calculate the elongation index and percentage of elongated cells. Cells with an elongation index of ≥ 2 were considered elongated. (I) Frequency distribution of long axis length for macrophages on $BCP_{<\mu m}$ and TCP. All continuous data presented as mean +SD of 3 donors in duplicate. **: $p < 0.01$, ***: $p < 0.001$.

2.9.2. Osteonectin staining and fluorescence intensity measurement

Formalin-fixed MSCs were stained with an antibody against osteonectin (ON, 1:5, AON-1, Developmental Studies Hydroma Bank) as a marker for osteoblast differentiation. The cells were processed for immunofluorescence as described above, using ON as primary antibody, a biotinylated secondary antibody (1:200, sheep anti-mouse biotinylated, RPN1001v1, GE Healthcare) and streptavidin Alexa Fluor 568 (5 μg/ml, Invitrogen) as tertiary antibody. The cell nuclei were stained with DAPI. Using the method described in by Shihan et al.,[71] fluorescent images taken with the 10× objective were processed for assessment of osteonectin mean fluorescence intensity, normalized to the number of cell nuclei in ImageJ.

2.10. Statistical analysis

Statistical analysis was performed using dedicated software tools (MS Excel, Microsoft, Albuquerque, NM, USA; GraphPad Prism, San Diego, CA, USA). Normal distribution of data was assessed by D'Agostino & Pearson normality test and normally distributed data were analyzed by parametric tests and non-normally distributed data by non-parametric tests. Cell shape measurements and ALP activity data were analyzed by Mann-Whitney *U* test, gene expression data by Friedman's test with Dunn's multiple comparisons test, protein level data by two-factor analysis of variance with Holm-Sidak's multiple comparisons test, angiogenic tube formation data and Osteonectin Mean Fluorescence Intensity by Welch's *t*-test. When protein levels in individual samples were below the detection limit of the standard curves in the assays, they were assigned a value of zero.

3. Results

3.1. Macrophages adopt an elongated morphology on submicron needle-shaped topography and mostly a spherical morphology on conventional surface structure

SEM of the material surfaces confirmed the presence of a topography consisting of submicron needle-shaped crystals on the surface of $BCP_{<\mu m}$, while TCP presented a relatively smooth surface with a globular topography (Fig. 2. A, B). After seeding, a large proportion of adherent macrophages on the submicron topography of $BCP_{<\mu m}$ adopted an elongated, bipolar shape, while on TCP the macrophages remained spherical (Fig. 2. C, D). Quantification of cell dimensions by measuring the short and long axes of macrophages on SEM images, indicated that the average short axis length was similar for both materials ($BCP_{<\mu m}$: 7.0 ± 3.9 μm; TCP: 5.7 ± 1.7 μm, $p = 0.4027$), while the average long axis length was substantially greater in macrophages adhering to $BCP_{<\mu m}$ versus TCP ($BCP_{<\mu m}$: 26.0 ± 13.5 μm; TCP: 8.4 ± 3.6 μm, $p < 0.001$) (Fig. 2. E, F). Consequently, the average elongation index was 3.5-fold greater for macrophages on $BCP_{<\mu m}$ than those on TCP ($BCP_{<\mu m}$: 5.2 ± 4.8; TCP: 1.5 ± 0.6 μm, $p < 0.001$) (Fig. 2. G). The percentage of elongated macrophages (elongation index ≥2) was also higher on $BCP_{<\mu m}$ compared to TCP, with 67.5% versus 15.4%, respectively (Fig. 2. H). Difference in long axis length between macrophages on the different materials was corroborated by a frequency distribution of the long axis length (Fig. 2. I).

3.2. Gene expression of adherent macrophages is influenced by bone substitute materials

To determine macrophage phenotype, expression of genes encoding for anti-inflammatory (*CD206*, *CD163*, *CCL18*) and for pro-inflammatory proteins (*CCL2*, *CCL5*, *IL1B*) was assessed in macrophages adherent to $BCP_{<\mu m}$ and TCP (Fig. 3). These genes were validated as markers for the respective phenotypes (Appendix Figure A1). Statistical analysis indicated overall statistical significance for *CD163* ($p < 0.0330$), *CCL18* ($p < 0.0330$), *CCL2* ($p < 0.0330$) and *IL1B* ($p < 0.0017$) data, but the post-hoc multiple comparisons tests did not reach significant differences between groups and timepoints.

3.3. Protein secretion and expression by macrophages varied between materials with submicron topography and conventional surface

To determine the phenotype of macrophages cultured on the bone graft materials, secretion of specific marker proteins was performed (Fig. 4). Based on literature and *in vitro* confirmation (Appendix Figure A2), production of the proteins CCL18 and sCD163 may be considered an indication for M2 macrophage polarization, while production of IL-6 and CCL5 indicate the M1 macrophage phenotype. Macrophages of all donors secreted the aforementioned cytokines in response to $BCP_{<\mu m}$ and TCP. Macrophages cultured on $BCP_{<\mu m}$ secreted higher levels of CCL18 than macrophages activated by TCP after both 24 h and 72 h. CCL18 levels were higher at 72 h compared to 24 h for both

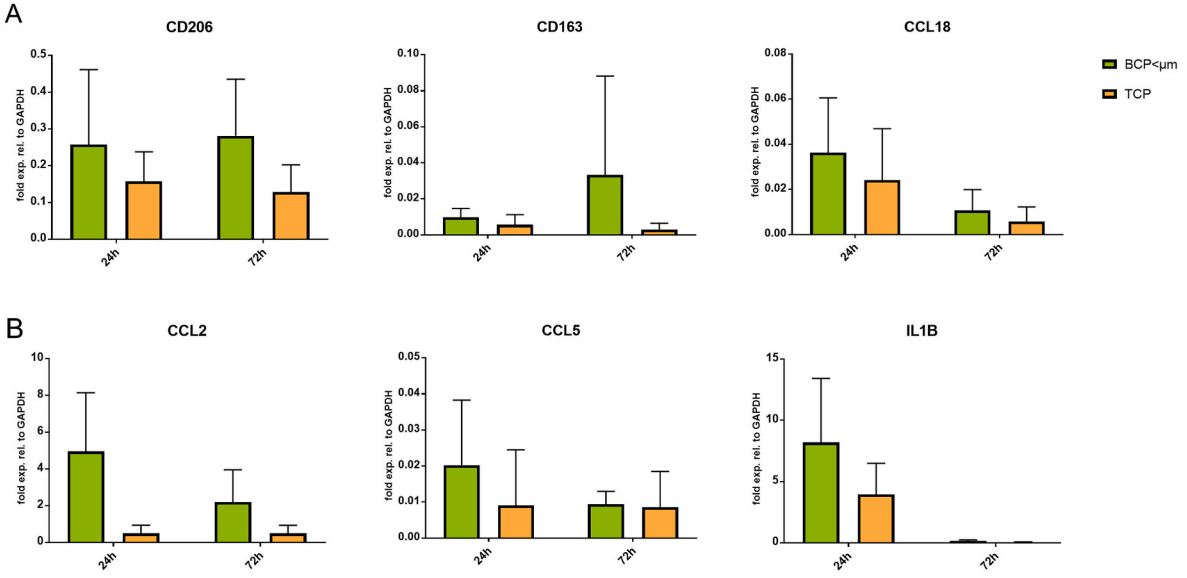

Fig. 3. Gene expression profiles of macrophages activated by $BCP_{<\mu m}$ and TCP. Quantification of gene expression of (A) M2 markers *CD206*, *CD163* and *CCL18*, and (B) M1 markers *CCL2*, *CCL5*, *IL1β* relative to *GAPDH* expression ($2^{-\Delta CT}$). Data represent mean +SD of a total of 3 separate monocyte donors in triplicate.

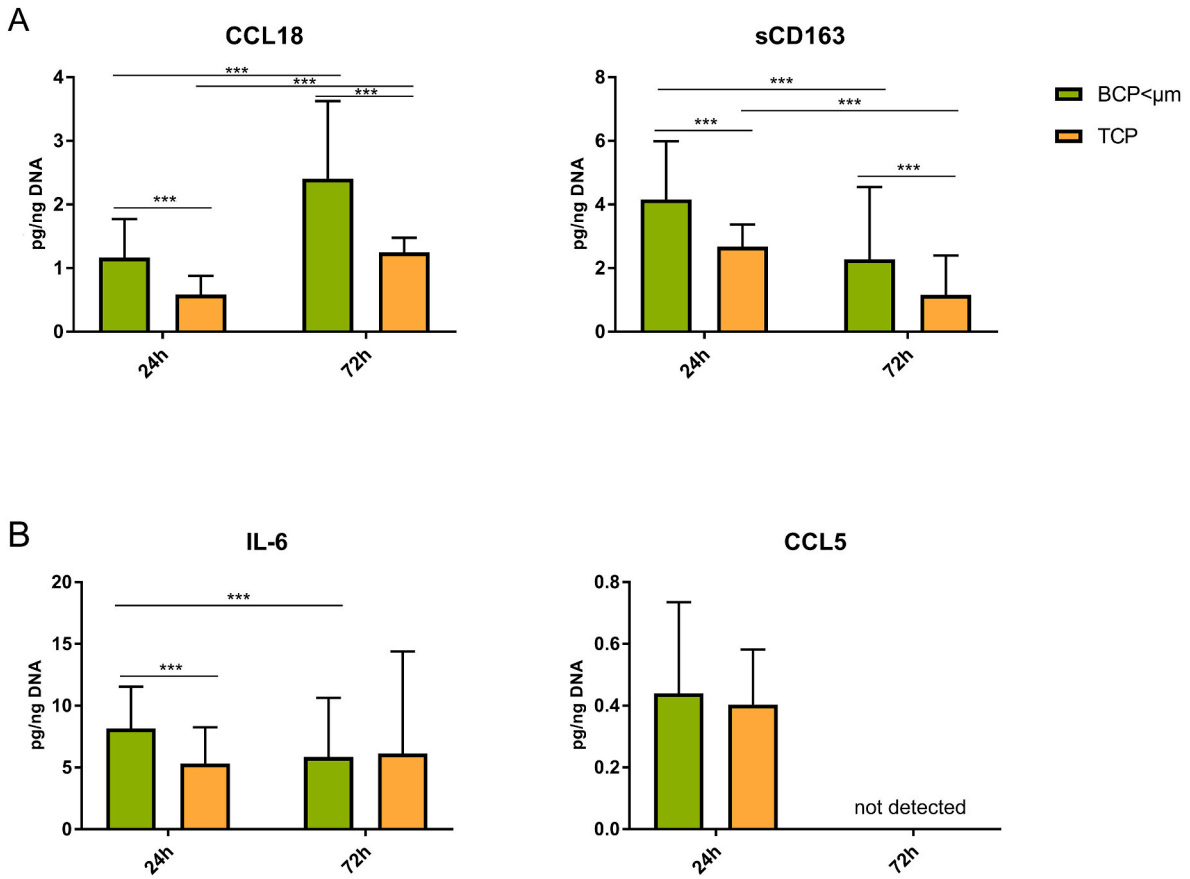

Fig. 4. Protein secretion of macrophages activated by BCP$_{<\mu m}$ and TCP. Measurement of (A) M2 markers CCL18 and CD163, and (B) M1 markers IL-6 and CCL5 in the culture medium of macrophages cultured on BCP$_{<\mu m}$ and TCP after 24 h and 72 h. Protein content was normalized to DNA content for each sample. Data represent mean +SD of a total of 4 separate donors in triplicate. ***:$p < 0.001$.

BCP$_{<\mu m}$ and TCP. Similarly, secretion of sCD163 by macrophages in response to BCP$_{<\mu m}$ was higher than the response to TCP after both 24 h and 72 h of culture. CD163 levels were lower at 72 h compared to 24 h for both BCP$_{<\mu m}$ and TCP. Secretion of IL-6 by macrophages cultured on BCP$_{<\mu m}$ was higher than the TCP condition after 24 h, but there was no difference between groups after 72 h because of a significant reduction in IL-6 levels on BCP$_{<\mu m}$. Protein levels of CCL5 were not different between conditions at 24 h, while undetectable at 72 h.

Macrophages adherent on BCP$_{<\mu m}$ and TCP were stained for CD68 (pan-macrophage marker), CD163 (anti-inflammatory macrophages), and iNOS (pro-inflammatory macrophages) (Fig. 5). Similar to observations by SEM, elongated macrophages were observed on the surface of BCP$_{<\mu m}$. Presence of CD68-positive cells (Fig. 5. A) on the surface of both BCP$_{<\mu m}$ and TCP confirmed that the observed adherent cells were macrophages. Likewise, CD163 signal (Fig. 5. B) was observed on most cells that were cultured on BCP$_{<\mu m}$ and TCP. iNOS (Fig. 5. C) was present in the majority of cells cultured on both materials. Overall, the observed cell density on TCP was lower than BCP$_{<\mu m}$.

3.4. Angiogenic tube formation and osteogenic differentiation are enhanced by macrophage activation by submicron topography

To assess whether bone graft material type influences paracrine signaling by adherent macrophages and its effect on angiogenesis, mCM of macrophages cultured on BCP$_{<\mu m}$ and TCP was used in a HUVEC tube formation assay (Fig. 6). After 16 h of incubation of HUVECs with mCM, angiogenic tube networks were more developed in the samples cultured with mCM from macrophages activated by BCP$_{<\mu m}$ (Fig. 6 A-C). Quantification of tube networks (Fig. 6. B, C) indicated that average tube length, number of tubes, and number of junctions was higher when exposed to conditioned medium of macrophages activated by BCP$_{<\mu m}$ than when exposed to TCP-mCM. BCP<µm and TCP controls without macrophages were equivalent in results of tube formation (data not shown).

In order to evaluate whether bone graft materials affect osteogenic paracrine signaling by adherent macrophages, BMSCs were exposed to mCM of macrophages cultured on BCP$_{<\mu m}$ or TCP during osteogenic differentiation. Osteogenic differentiation was determined by assessing activity of ALP and expression of osteonectin in BMSCs[69,72] (Fig. 7). After 10 days, ALP activity in BMSCs was not significantly different between BCP$_{<\mu m}$-mCM and TCP-mCM, with ALP normalized to DNA of MSCs (Fig. 7. A). When ALP activity in MSCs was also normalized to the DNA of macrophages cultured on BCP$_{<\mu m}$ and TCP, a moderate but statistically significant difference was found between the bone substitute grafts, in favor of BCP$_{<\mu m}$ (Fig. 7. B). Controls of BCP$_{<\mu m}$ and TCP without macrophages did not lead to significant differences in ALP activity (data not shown). Osteogenic differentiation of MSCs was further confirmed by immunostaining for osteonectin as an additional marker for osteogenic differentiation. Osteonectin-positive cells were observed in conditions with both BCP$_{<\mu m}$-mCM and TCP-mCM (Fig. 7. D). Quantification of osteonectin fluorescence intensity normalized to cell number revealed a higher expression of osteonectin in macrophages on BCP$_{<\mu m}$ (Fig. 7. C).

4. Discussion

In this study, we have shown differential responses of primary human macrophages cultured on calcium phosphate materials with

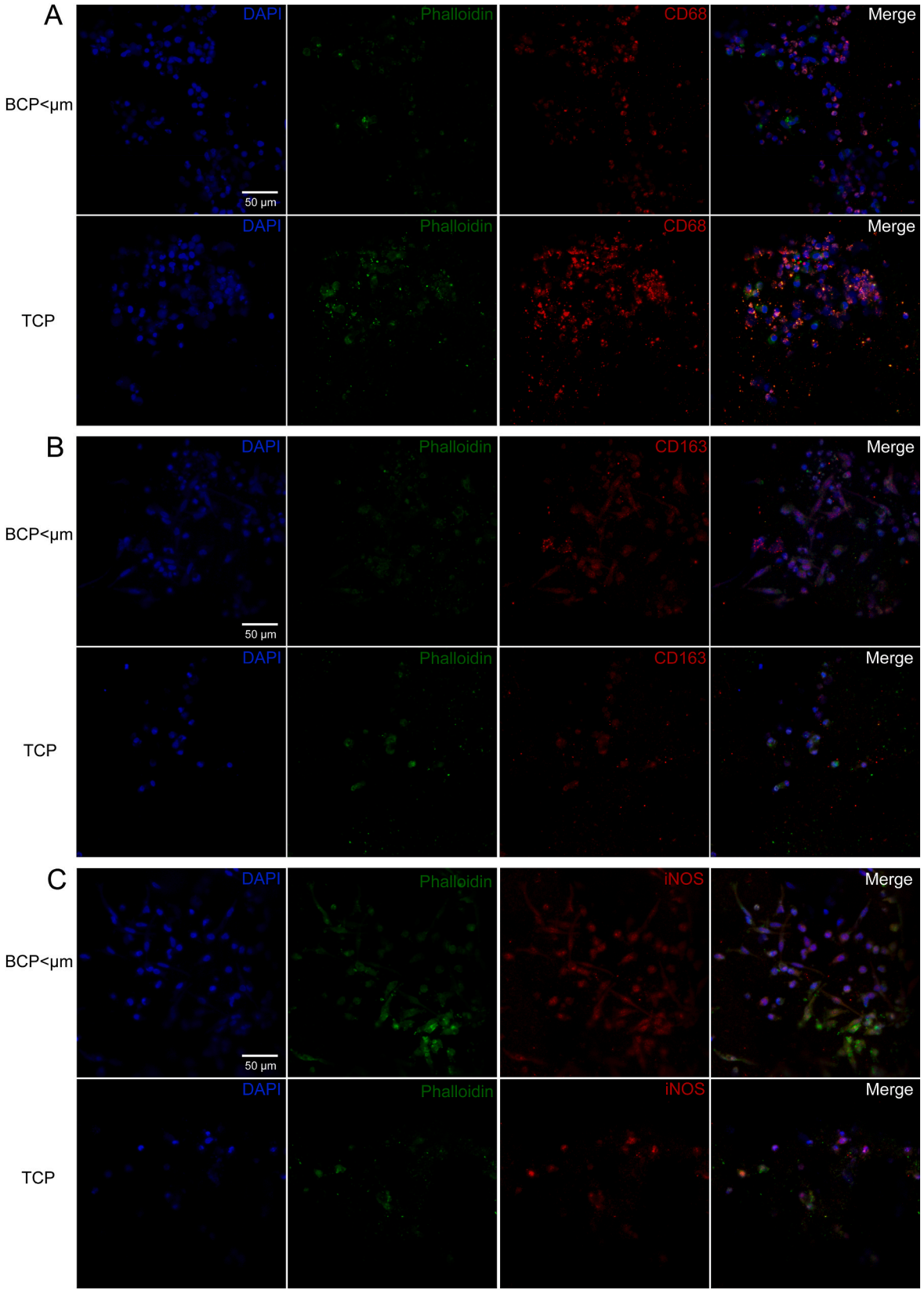

Fig. 5. Immunofluorescent phenotypic marker expression by macrophages cultured on calcium phosphates. Representative confocal microscopy images of macrophages cultured on $BCP_{<\mu m}$ and TCP immunostained for (A) CD68 (pan-macrophage marker), (B) CD163 (anti-inflammatory), and (C) iNOS (pro-inflammatory). Cells were counterstained with phalloidin to visualize the cytoskeleton (F-actin) and DAPI as a nuclear staining.

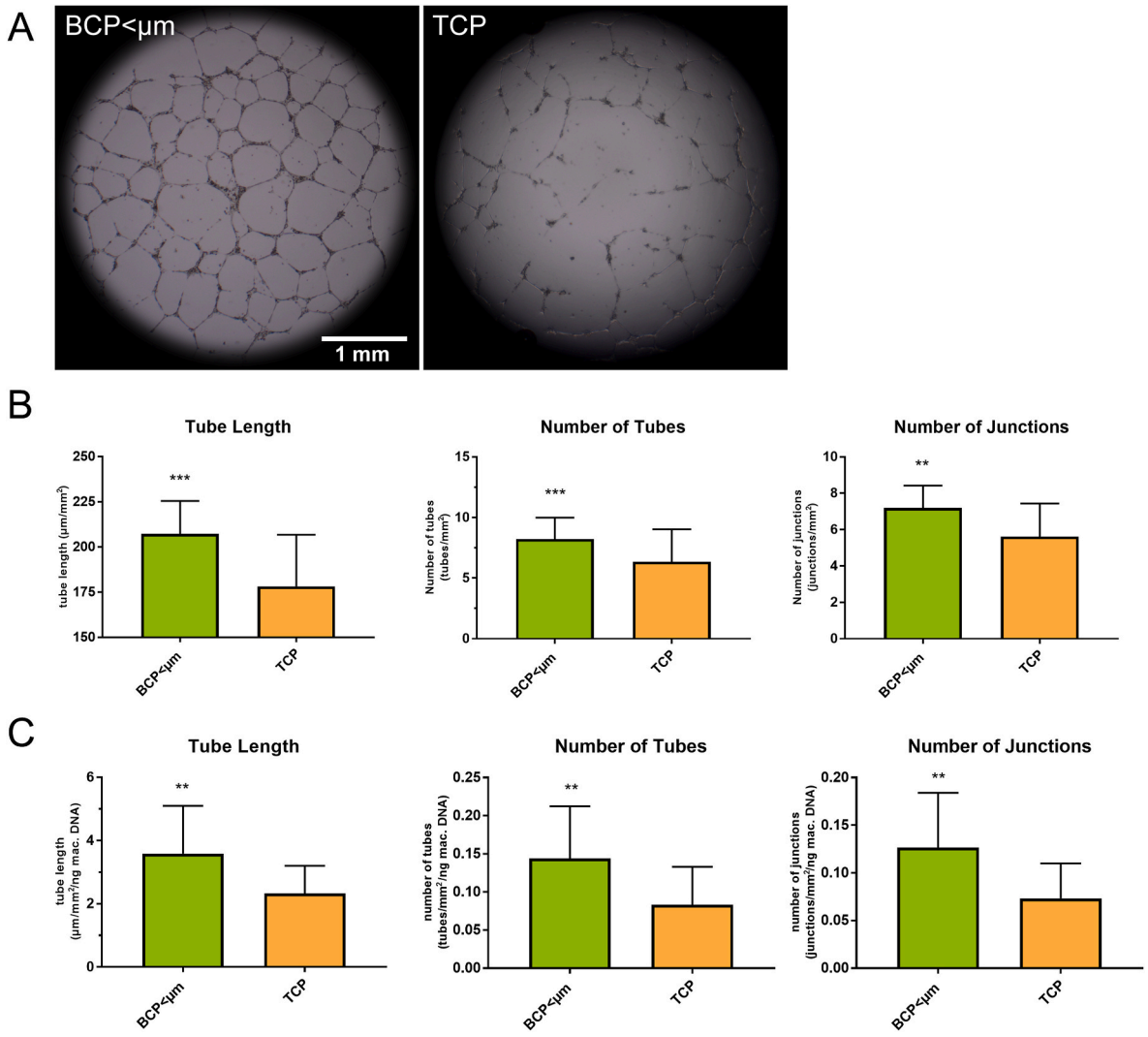

Fig. 6. Endothelial tube formation assay with medium conditioned by macrophages cultured on calcium phosphates. (A) Representative microscopy images of endothelial tube networks formed by HUVECs after 16 h incubation with conditioned medium of macrophages cultured on $BCP_{<\mu m}$ or TCP. (B) Results of tube network quantification, measuring tube length, number of tubes and number of junctions per mm^2. (C) Results of tube network quantification normalized to macrophage DNA. Data represent mean +SD of a total of 3 separate monocyte donors. **: $p < 0.01$, ***: $p < 0.001$.

different surface topographies. Macrophages cultured on the submicron topography of $BCP_{<\mu m}$ were found to have an elongated morphology compared to macrophages cultured on TCP. Protein and gene expression analyses demonstrated higher expression of M1 and M2 markers of macrophages cultured on $BCP_{<\mu m}$, indicating an overall stronger activation of macrophages. The protein data revealed a phenotypic skewing of macrophages towards the M2 phenotype on $BCP_{<\mu m}$ *versus* TCP after 72 h. Lastly, medium conditioned by macrophages cultured on $BCP_{<\mu m}$ also enhanced angiogenic tube formation by HUVECs and osteogenic differentiation of MSCs compared to medium conditioned by macrophages cultured on TCP.

The efficacy of biomaterials is dependent on their material properties and the associated initial cell and tissue responses following implantation. Macrophages are among the first cells to colonize an implant and as key regulators of the healing cascade, their response to implant materials is pivotal for healing outcomes.[28–31,33] Here, the first material ($BCP_{<\mu m}$) was of biphasic composition, had a submicron topography of needle-shaped crystals with previously demonstrated potential to form bone in soft tissues[9] and high bone healing capacity *in vivo*.[12,15,18] The second material, TCP, had a smooth surface, was not osteoinductive[53] and had relatively low bone healing potential.[11,12,54,55]

The observation of elongated macrophage morphology on $BCP_{<\mu m}$ corroborates the suggestion of M2 macrophage activation. In literature, various groups have demonstrated associations between elongated macrophage morphology and M2-like activation.[73–80] For example, McWhorter et al. determined that murine bone marrow-derived macrophages adopted an elongated morphology *in vitro* after treatment with IL-4/IL-13, which induced an arginase-1-positive, iNOS-negative M2 phenotype.[77] Moreover, several studies have shown that forcing macrophage elongation by physical cues, such as micropatterned surfaces,[76,77] microfiber scaffolds,[78] and magnetic fields,[79] resulted in polarization towards an M2 phenotype.[76–79] A recent study by Tylek et al. demonstrated that melt-electrowritten fiber scaffolds with defined pore sizes induced elongation of primary human macrophages *in vitro*. Phenotype characterization revealed that the elongated macrophages were M2-activated, as evidenced by gene expression (downregulation of M1 markers *IL1B* and *IL8*; upregulation of M2 markers *CD206*, *CD163* and *IL10*) and protein markers (downregulation of M1 markers IL-1β, IL-8 and IL-6; upregulation of M2 marker IL-10) [74]. In the current study, we also determined upregulation of M2 markers at gene (*CD206*) and protein level (CCL18, sCD163) for elongated macrophages on $BCP_{<\mu m}$, although we did not observe downregulation of M1 markers in a similar manner. This may be related to the substantially greater length of elongated macrophages reported by Tylek et al. Alternatively, it may

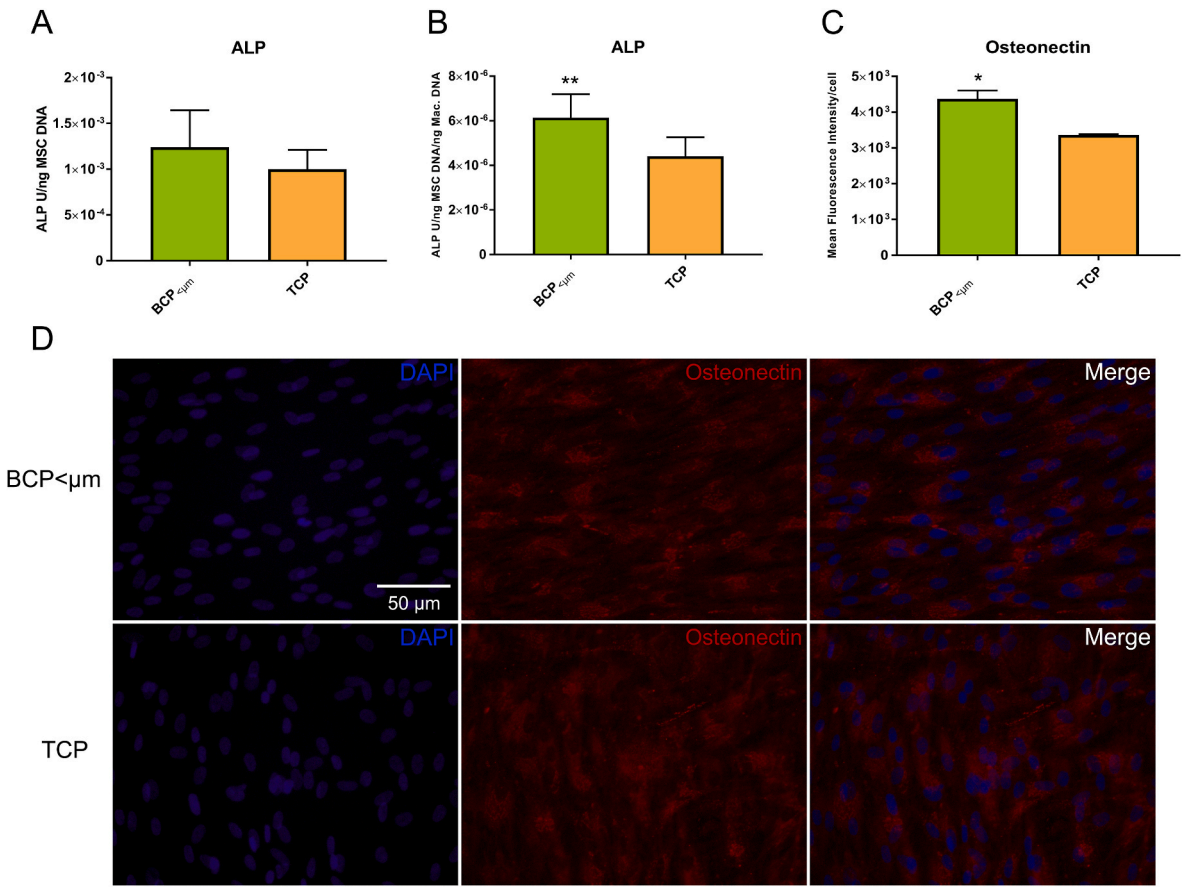

Fig. 7. Osteogenic differentiation of MSCs with medium conditioned by macrophages cultured on calcium phosphates. (A,B) Quantification of ALP activity in MSCs after 10 days of culture in osteogenic differentiation medium with $BCP_{<\mu m}$-mCM and TCP-mCM. Data are shown as (A) ALP activity normalized to MSC DNA and (B) normalized to MSC DNA and macrophage DNA. (C) Mean fluorescence intensity of osteonectin marker on microscopy images of MSCs differentiated in $BCP_{<\mu m}$-mCM and TCP-mCM, normalized to number of cells. Data represent mean +SD of a total of 3 separate monocyte donors. (D) Microscopy images of differentiated MSCs stained for osteonectin and DAPI. *: $p < 0.05$, **: $p < 0.01$.

be an effect of the different materials used, as we used calcium phosphate and that study used fiber scaffolds of poly (ε-caprolactone). It is interesting to note that we did not observe a difference in expression of iNOS and CD163 by immunofluorescence between elongated and spherical macrophages (Fig. 5). However, McWhorter et al. reported a similar observation that iNOS expression was not altered in micropatterning-induced elongated murine macrophages, even though pro-inflammatory cytokine release was reduced and M2 markers were augmented.[77] Taken together, the literature is clear that macrophage elongation is associated with the M2 phenotype which confirms the observations in the current work.

Interesting questions with the observed macrophage elongation are why and how macrophages take on an elongated shape on $BCP_{<\mu m}$ and what is its involvement in the observed M2 phenotype skewing. McWhorter et al. demonstrated an essential role of the actin cytoskeleton in shape-induced M2 macrophage polarization, as treatment of the cells with various pharmacological inhibitors of the actin cytoskeleton dynamics, *i.e.* actin polymerization and actin/myosin contractility, resulted in loss of M2 phenotype.[77] Likewise, Zhu et al. reported that RAW 264.7 macrophage M2 polarization on TiO_2 honeycomb surface topography was associated with upregulation of the Rho family of GTPases, which are regulators of the actin cytoskeleton.[81] Yet another study by Yang et al. also reported that M2 macrophage activation by titanium 'micro/nano-net' surface topography was associated with enhanced Rho-associated protein kinase (ROCK) expression and reduced Src expression, which are key up-regulators and down-regulators of actin cytoskeletal tension, respectively.[82,83] These studies demonstrate that topographical features of materials can modulate macrophage shape and induce cytoskeletal rearrangements, which play a role in M2 macrophage phenotype upregulation. It is widely accepted that cell shape can influence downstream signaling and cell behavior through various mechanotransduction pathways.[84] By these means, the submicron needle-shaped topography of $BCP_{<\mu m}$ may lead to M2 activation through cell shape modulation and mechanotransduction[85] . Further studies are needed to elucidate the precise mechanisms of macrophage elongation on biomaterial topographies and its involvement in macrophage polarization.

Compared to macrophages polarized to the M1 and M2 phenotype on tissue culture polystyrene using cytokines (Supplementary Fig. 1, 2), the macrophages on $BCP_{<\mu m}$ and TCP were significantly less 'polarized'. The concurrent expression of both M1 and M2 protein and gene markers in macrophages cultured on the bone graft materials, could indicate presence of either a 'mixed', heterogeneous population of polarized M1-and M2-like macrophages, or an 'intermediate' macrophage phenotype on the spectrum in between M1 and M2. Because immunohistochemistry for M1 (iNOS) and M2 (CD163) markers at 72 h revealed presence of both markers in the majority of macrophages on $BCP_{<\mu m}$ and TCP, this may indeed suggest that a 'mixed', intermediate macrophage phenotype was observed. However, it may be argued that the cytokine-polarized macrophages phenotypes in the control conditions are an extreme condition that is difficult to achieve without presence of these cytokines in high concentrations. It has been long recognized that instead of the reductionist M1/M2 macrophage classification, macrophages exist on a spectrum between these phenotypic poles and there are myriad

intermediate subtypes.[30,86–88] The protein data and cell shape data of the current study suggest a subtle skewing of macrophages towards an M2-like phenotype on $BCP_{<\mu m}$ compared to TCP.

As our results indicate phenotypic skewing of human macrophages towards an M2-like phenotype on $BCP_{<\mu m}$ *in vitro*, we may speculate on the relevance of these findings to bone regeneration with calcium phosphate bone substitutes *in vivo*. We know from previous studies with animal models that $BCP_{<\mu m}$, and other submicron surface-structured calcium phosphates, have greater bone regenerative capacity than conventional calcium phosphates without submicron surface structure.[8,9,11,12,53] Recently, in a study similar to the current work, Li et al. demonstrated elevated M2-like activation (CD206, *Arg-1*, *VEGF*, VEGF, *IGF-1*, IGF-1) of murine RAW 264.7 macrophages on osteoinductive β-TCP with submicron surface structure, while β-TCP with micron surface structure induced an M1-like phenotype (*iNOS*, iNOS, TNF-α, *IL6*, IL-6, IL-1β, *IL1B*).[51] In a similar study using THP-1 macrophages, we have previously also determined M2 activation (CCL18, TGF-β) on osteoinductive TCP with submicron surface structure and M1-activation (TNF-α, IL-1β) on micron surface structure *in vitro*[89] . Yet another study by Chen et al. determined upregulation of M2 markers (*Arg-1*, CD206, IL-10, IGF) in RAW 264.7 macrophages cultured on BCP with high osteoinductive potential versus HA and β-TCP with lower osteoinductive potential, which exhibited greater M1-like activation (CCR7, iNOS, IL-1β, TNF-α, CCL2).[52] Both studies moved on to evaluate macrophage phenotypes in association with these materials after intramuscular implantation in mice. Both reported a greater population of anti-inflammatory, M2-like macrophages around the osteoinductive materials that induced ectopic bone formation, while more M1-like macrophages were observed around materials that did not induce ectopic bone formation.[51,52] Likewise, we have previously found higher levels of anti-inflammatory factor IL-10 around osteoinductive versus non-inductive TCP after ectopic implantation in canines, suggesting presence of anti-inflammatory macrophages.[89] Our current *in vitro* findings, together with *in vivo* results previously obtained with $BCP_{<\mu m}$, are in agreement with the findings of the aforementioned studies. However, as opposed to the results of these other studies, we did not observe enhanced M1 macrophage activation on the material without submicron surface topography. This observation may be due to different *in vitro* culture conditions or may be species-related, since to our current knowledge, this study was the first to evaluate macrophage response to calcium phosphate with submicron surface topography using primary macrophages from humans. Naturally, primary macrophages cultured *in vitro* are considered a more representative model of the human immune response as compared to murine macrophages or human monocytic cell lines. While the exact mechanism of M2 macrophage contribution to bone regeneration by calcium phosphates remains to be elucidated, evidence for their involvement has so far been congruent.

Angiogenesis and osteogenic differentiation of stem cells are critical processes during bone healing. Ingrowing blood vessels are needed to provide essential nutrients and are a source of stem cells (i.e. pericytes), while stem cell differentiation provides bone-forming cells. *In vitro* outcomes of angiogenic tube formation by HUVECs and osteogenic differentiation of MSCs have been shown to be predictive of *in vivo* effects.[69,90,91] The enhanced angiogenic tube formation by HUVECs and subtle increase in osteogenic differentiation of MSCs after exposure to $BCP_{<\mu m}$-mCM, suggest an altered or upregulated paracrine signaling by macrophages on $BCP_{<\mu m}$ that is indicative of a pro-healing, M2-like functional phenotype. Previous research has demonstrated that macrophages exhibit intricate crosstalk with endothelial cells during angiogenesis and vascularization.[58,92,93] Similarly, macrophages are involved in bone healing through communication with MSCs and pre-osteoblasts by paracrine signaling factors.[37,94] Other studies that have evaluated effects of macrophages in *in vitro* angiogenic tube formation[44,89,95–99] and osteogenic differentiation assays[44,51,52,94,98] have associated upregulated angiogenic and osteogenic responses with anti-inflammatory M2-activated macrophages. These findings further support our observation M2 macrophage upregulation on $BCP_{<\mu m}$ and suggest involvement of M2 macrophages in the enhanced bone healing observed with calcium phosphates with submicron topography *in vivo*.

A limitation of the current study is that the calcium phosphate bone graft materials that were compared were not different only in topographical features, but also in chemistry. TCP has a higher solubility than HA, which translates to a higher release of Ca and P ions for TCP than BCP.[9,53] This could be a potential confounder for the effect of topography on the results obtained in this study, because different concentrations of ionic Ca and P could ultimately influence macrophage response. Some studies have shown that surface chemistry of calcium phosphate can influence the total amount and type of proteins adsorbed to the material surface, which is dependent on the ratio of available Ca and P sites that have differential affinity for protein adsorption.[100] In this way, chemistry may influence cell-surface interactions and subsequent cell behavior. However, various studies have previously demonstrated that topography of calcium phosphates has a stronger effect on protein adsorption than chemistry.[81,101] For example, previous studies have isolated chemical and topographical effects of calcium phosphates by coating the surface of materials with metal (i.e. gold, titanium), thereby inhibiting ion dissolution at the surface.[101–104] Using this approach, Engel et al. concluded that topographical effects are dominant over chemical effects of calcium phosphates on cells *in vitro*.[103] Likewise, Davison et al. demonstrated that, compared to uncoated controls, titanium-coated calcium phosphate did not differentially affect *in vitro* osteoclastogenesis of RAW264.7 macrophages and osteoinductive potential of the materials *in vivo*, thereby also indicating a dominant effect of topography.[102] Other studies have previously shown that there is no correlation between *in vitro* ion release by calcium phosphates and *in vivo* osteoinductive potential, whereas this relationship has been clearly established for surface topography.[9,53] In a similar study compared to the current work, Chen et al. suggested that phase composition of calcium phosphates was the driving factor in polarization of RAW 264.7 macrophages *in vitro*, showing an M2-dominant response on BCP and an M1-dominant response on β-TCP.[52] However, the authors may have overlooked the influence of surface topography, as they did acknowledge that the surface grain size for β-TCP was over 3-fold greater than for BCP, while they failed to demonstrate a difference in Ca and P release between the two materials *in vitro*. Other studies have also demonstrated a clear effect of material topography on macrophage response by using calcium phosphates with identical chemistry and different topography, or insoluble materials such as titanium and polymers.[51,105–107] Lastly, in the current work, material-only conditioned medium controls of $BCP_{<\mu m}$ and TCP produced no differences in both the tube formation and osteogenic differentiation assays, which indicate that potential differences in ion concentrations did not directly affect the cells in these assays (data not shown). Taken together, the influence of substrate chemistry seems to be of lower importance than substrate topography. However, future studies on materials with identical chemistry and different topography are recommended. Other study limitations are related to the nature of every *in vitro* study, including limitations of assessment techniques, markers and timepoints, as well as the predictive potential for *in vivo* outcomes. Fortunately, various previous studies have already demonstrated a correlation between *in vitro* and *in vivo* macrophage phenotype in response to biomaterials, and their *in vivo* bone healing outcomes.[44,51,52,83] Lastly, in the current study, we were unable to quantify immunofluorescent marker (CD163, iNOS) intensity due to variable cell densities and uneven surfaces of the materials. Although the observed cell density at the surface of TCP appeared lower than $BCP_{<\mu m}$, this was most probably the result of cell detachment from TCP during storage and handling for immunofluorescent staining, because DNA assays did not indicate a difference in cell number between groups (data not shown).

5. Conclusion

This *in vitro* study has found an overall stronger macrophage activation and subtle shift towards an M2-like macrophage phenotype on calcium phosphate with submicron topography, compared to calcium phosphate without submicron topography. Enhanced pro-regenerative paracrine signaling to (stem) cells by macrophages on calcium phosphate with submicron topography was determined in angiogenic and osteogenic assays. These findings, in line with findings from other studies, suggest that M2 macrophage upregulation may play a role in the enhanced bone regeneration capacity of calcium phosphates with submicron topography. Immunomodulation through biomaterial surface topography is indicated as a strategy to be further explored for improvement of tissue regeneration using biomaterials.

Authorship contribution statement

LvD: Conceptualization and study design, experimental work, data analysis, writing - original draft. LU: Conceptualization and study design, experimental work, writing – reviewing and editing. HY: Material preparation and characterization, writing – reviewing and editing. FBdG: Supervision, Conceptualization and study design, writing – reviewing and editing. DG: Supervision, conceptualization and study design, writing – reviewing and editing. AR: Supervision, writing – reviewing and editing. JdB: Supervision, writing – reviewing and editing

Declaration of competing interest

The authors declare the following financial interests/personal relationships which may be considered as potential competing interests: Lukas A van Dijk reports a relationship with Kuros Biosciences BV that includes: employment. Florence de Groot reports a relationship with Kuros Biosciences BV that includes: employment. Huipin Yuan reports a relationship with Kuros Biosciences BV that includes: employment and equity or stocks. Joost de Bruijn reports a relationship with Kuros Biosciences BV that includes: board membership, employment, and equity or stocks. Joost de Bruijn, Florence de Groot has patent issued to Kuros Biosciences BV.

Data availability

Data will be made available on request.

Acknowledgements

This study was supported by the European Union's Horizon 2020 research and innovation program (grant agreements no. 674282, no. 874790 and no. 953169).

Appendix A. Supplementary data

Supplementary data related to this article can be found at https://doi.org/10.1016/j.regen.2023.100070.

References

1 Eliaz N, Metoki N. Calcium phosphate bioceramics: a review of their history, structure, properties, coating technologies and biomedical applications. *Materials*. 2017. https://doi.org/10.3390/ma10040334.
2 Fariña NM, Guzón FM, Peña ML, Cantalapiedra AG. In vivo behaviour of two different biphasic ceramic implanted in mandibular bone of dogs. *J Mater Sci Mater Med*. 2008, 191565–1573.
3 Jensen SS, Bornstein MM, Dard M, Bosshardt DD, Buser D. Comparative study of biphasic calcium phosphates with different HA/TCP ratios in mandibular bone defects. A long-term histomorphometric study in minipigs. *J Biomed Mater Res Part B Appl. Biomater.* 2009;90 B:171–181.
4 Yuan H, Van Blitterswijk CA, De Groot K, De Bruijn JD. A comparison of bone formation in biphasic calcium phosphate (BCP) and hydroxyapatite (HA) implanted in muscle and bone of dogs at different time periods. *J Biomed Mater Res*. 2006;78:139–147.
5 Eggli PS, Muller W, Schenk RK. Porous hydroxyapatite and tricalcium phosphate cylinders with two different pore size ranges implanted in the cancellous bone of rabbits. A comparative histomorphometric and histologic study of bone ingrowth and implant substitution. *Clin Orthop Relat Res*. 1988:127–138.
6 Galois L, Mainard D. Bone ingrowth into two porous ceramics with different pore sizes: an experimental study. *Acta Orthop Belg*. 2004;70:598–603.
7 Gauthier O, Bouler JM, Aguado E, Pilet P, Daculsi G. Macroporous biphasic calcium phosphate ceramics: influence of macropore diameter and macroporosity percentage on bone ingrowth. *Biomaterials*. 1998;19:133–139.
8 Duan R, Barbieri D, De Groot F, De Bruijn JD, Yuan H. Modulating bone regeneration in rabbit condyle defects with three surface-structured tricalcium phosphate ceramics. *ACS Biomater Sci Eng*. 2018;4:3347–3355.
9 Duan R, van Dijk LA, Barbieri D, de Groot F, Yuan H, de Bruijn JD. Accelerated bone formation by biphasic calcium phosphate with a novel sub-micron surface topography. *Eur Cell Mater*. 2019;37:60–73.
10 Yuan H, Fernandes H, Habibovic P, et al. Osteoinductive ceramics as a synthetic alternative to autologous bone grafting. *Proc Natl Acad Sci USA*. 2010;107:13614–13619. U. S. A.
11 Barbieri D, Yuan H, Ismailoğlu AS, De Bruijn JD. Comparison of two moldable calcium phosphate-based bone graft materials in a noninstrumented canine interspinous implantation model. *Tissue Eng*. 2017;23:1310–1320.
12 Van Dijk LA, Barrère-De Groot F, Rosenberg AJWP, et al. MagnetOs, Vitoss, and novabone in a multi-endpoint study of posterolateral fusion: a true fusion or not? *Clin. Spine Surg*. 2020;33:E276–E287.
13 Duan R, Barbieri D, Luo X, Weng J, de Bruijn JD, Yuan H. Submicron-surface structured tricalcium phosphate ceramic enhances the bone regeneration in canine spine environment. *J Orthop Res*. 2016;34:1865–1873.
14 Habibovic P, Yuan H, van den Doel M, Sees TM, van Blitterswijk CA, de Groot K. Relevance of osteoinductive biomaterials in critical-sized orthotopic defect. *J Orthop Res*. 2006;24:867–876.
15 van Dijk LA, Duan R, Luo X, et al. Biphasic calcium phosphate with submicron surface topography in an Ovine model of instrumented posterolateral spinal fusion. *JOR Spine*. 2018;1, e1039.
16 Habibovic P, Yuan H, Van Der Valk CM, Meijer G, Van Blitterswijk CA, De Groot K. 3D microenvironment as essential element for osteoinduction by biomaterials. *Biomaterials*. 2005;26:3565–3575.
17 Barradas AMC, Yuan H, van Blitterswijk CA, Habibovic P. Osteoinductive biomaterials: current knowledge of properties, experimental models and biological mechanisms. *Eur Cell Mater*. 2011. https://doi.org/10.22203/eCM.v021a31.
18 van Dijk LA, Barbieri D, Barrère-de Groot F, et al. Efficacy of a synthetic calcium phosphate with submicron surface topography as autograft extender in lapine posterolateral spinal fusion. *J Biomed Mater Res Part B Appl. Biomater.* 2019;107:2080–2090.
19 Chung L, Maestas DR, Housseau F, Elisseeff JH. Key players in the immune response to biomaterial scaffolds for regenerative medicine. *Adv Drug Deliv Rev*. 2017. https://doi.org/10.1016/j.addr.2017.07.006.
20 Morais JM, Papadimitrakopoulos F, Burgess DJ. Biomaterials/tissue interactions: possible solutions to overcome foreign body response. *AAPS J*. 2010. https://doi.org/10.1208/s12248-010-9175-3.
21 Julier Z, Park AJ, Briquez PS, Martino MM. Promoting tissue regeneration by modulating the immune system. *Acta Biomater*. 2017. https://doi.org/10.1016/j.actbio.2017.01.056.
22 Brown BN, Ratner BD, Goodman SB, Amar S, Badylak SF. Macrophage polarization: an opportunity for improved outcomes in biomaterials and regenerative medicine. *Biomaterials*. 2012. https://doi.org/10.1016/j.biomaterials.2012.02.034.
23 Davenport Huyer L, Pascual-Gil S, Wang Y, Mandla S, Yee B, Radisic M. Advanced strategies for modulation of the material–macrophage interface. *Adv Funct Mater*. 2020;30, 1909331.
24 Mantovani A, Biswas SK, Galdiero MR, Sica A, Locati M. Macrophage plasticity and polarization in tissue repair and remodelling. *J Pathol*. 2013. https://doi.org/10.1002/path.4133.
25 Mosser DM, Edwards JP. Exploring the full spectrum of macrophage activation. *Nat Rev Immunol*. 2008. https://doi.org/10.1038/nri2448.
26 Murray PJ, Allen JE, Biswas SK, et al. Macrophage activation and polarization: nomenclature and experimental guidelines. *Immunity*. 2014;41:14–20.
27 Taraballi F, Sushnitha M, Tsao C, et al. Biomimetic tissue engineering: tuning the immune and inflammatory response to implantable biomaterials. *Adv. Healthc. Mater*. 2018. https://doi.org/10.1002/adhm.201800490.
28 Wynn TA, Vannella KM. Immunity. In: *Macrophages in Tissue Repair, Regeneration, and Fibrosis*. Cell Press; 2016. March 15.
29 Chen Z, Klein T, Murray RZ, et al. Osteoimmunomodulation for the development of advanced bone biomaterials. *Mater Today*. 2016. https://doi.org/10.1016/j.mattod.2015.11.004.
30 Klopfleisch R. Macrophage reaction against biomaterials in the mouse model – phenotypes, functions and markers. *Acta Biomater*. 2016;43:3–13.
31 Klopfleisch R, Jung F. The pathology of the foreign body reaction against biomaterials. *J Biomed Mater Res, Part A*. 2017. https://doi.org/10.1002/jbm.a.35958.
32 Horwood NJ. Macrophage polarization and bone formation: a review. *Clin Rev Allergy Immunol*. 2016. Humana Press Inc., August 1.
33 Miron RJ, Bosshardt DD. OsteoMacs: key players around bone biomaterials. *Biomaterials*. 2016;82:1–19.

34 Alexander KA, Chang MK, Maylin ER, et al. Osteal macrophages promote in vivo intramembranous bone healing in a mouse tibial injury model. *J Bone Miner Res*. 2011.
35 Raggatt LJ, Wullschleger ME, Alexander KA, et al. Fracture healing via periosteal callus formation requires macrophages for both initiation and progression of early endochondral ossification. *Am J Pathol*. 2014. https://doi.org/10.1016/j.ajpath.2014.08.017.
36 Humbert P, Brennan M, Davison N, et al. Immune modulation by transplanted calcium phosphate biomaterials and human mesenchymal stromal cells in bone regeneration. *Front Immunol*. 2019. https://doi.org/10.3389/fimmu.2019.00663.
37 Pajarinen J, Lin T, Gibon E, et al. Mesenchymal stem cell-macrophage crosstalk and bone healing. *Biomaterials*. 2019. https://doi.org/10.1016/j.biomaterials.2017.12.025.
38 Zhang R, Liang Y, Wei S. M2 macrophages are closely associated with accelerated clavicle fracture healing in patients with traumatic brain injury: a retrospective cohort study. *J Orthop Surg Res*. 2018;13:213.
39 Shi S, Zhang Q, Atsuta I, et al. IL-17-mediated M1/M2 macrophage alteration contributes to pathogenesis of bisphosphonate-related osteonecrosis of the jaws. *Clin Cancer Res*. 2013;19:3176–3188.
40 Wehrhan F, Moebius P, Amann K, et al. Macrophage and osteoclast polarization in bisphosphonate associated necrosis and osteoradionecrosis. *J Cranio-Maxillofacial Surg*. 2017;45:944–953.
41 Zhu W, Xu R, Du J, et al. Zoledronic acid promotes TLR-4-mediated M1 macrophage polarization in bisphosphonate-related osteonecrosis of the jaw. *Faseb J*. 2019;33:5208–5219.
42 Castaño IM, Raftery RM, Chen G, et al. Rapid bone repair with the recruitment of CD206+M2-like macrophages using non-viral scaffold-mediated miR-133a inhibition of host cells. *Acta Biomater*. 2020. https://doi.org/10.1016/j.actbio.2020.03.042.
43 Hachim D, LoPresti ST, Yates CC, Brown BN. Shifts in macrophage phenotype at the biomaterial interface via IL-4 eluting coatings are associated with improved implant integration. *Biomaterials*. 2017. https://doi.org/10.1016/j.biomaterials.2016.10.019.
44 Mahon OR, Browe DC, Gonzalez-Fernandez T, et al. Nano-particle mediated M2 macrophage polarization enhances bone formation and MSC osteogenesis in an IL-10 dependent manner. *Biomaterials*. 2020;239, 119833.
45 Zhang J, Shi H, Zhang N, Hu L, Jing W, Pan J. Interleukin-4-loaded hydrogel scaffold regulates macrophages polarization to promote bone mesenchymal stem cells osteogenic differentiation via TGF-β1/Smad pathway for repair of bone defect. *Cell Prolif*. 2020. https://doi.org/10.1111/cpr.12907.
46 Zhao DW, Zuo KQ, Wang K, et al. Interleukin-4 assisted calcium-strontium-zinc-phosphate coating induces controllable macrophage polarization and promotes osseointegration on titanium implant. *Mater Sci Eng, C*. 2021. https://doi.org/10.1016/j.msec.2020.111512.
47 Zheng Z wei, hong Chen Y, Wu D yu, et al. Development of an accurate and proactive immunomodulatory strategy to improve bone substitute material-mediated osteogenesis and angiogenesis. *Theranostics*. 2018;8:5482–5500.
48 Bohner M, Miron RJ. A proposed mechanism for material-induced heterotopic ossification. *Mater Today*. 2019;22:132–141.
49 Olmsted-Davis E, Mejia J, Salisbury E, Gugala Z, Davis AR. A population of M2 macrophages associated with bone formation. *Front Immunol*. 2021;12:1.
50 Davison NL, Gamblin AL, Layrolle P, Yuan H, de Bruijn JD, Barrère-de Groot F. Liposomal clodronate inhibition of osteoclastogenesis and osteoinduction by submicrostructured beta-tricalcium phosphate. *Biomaterials*. 2014;35:5088–5097.
51 Li M, Guo X, Qi W, et al. Macrophage polarization plays roles in bone formation instructed by calcium phosphate ceramics. *J Mater Chem B*. 2020;8:1863–1877.
52 Chen X, Wang M, Chen F, et al. Correlations between macrophage polarization and osteoinduction of porous calcium phosphate ceramics. *Acta Biomater*. 2020;103:318–332.
53 Duan R, Barbieri D, Luo X, et al. Variation of the bone forming ability with the physicochemical properties of calcium phosphate bone substitutes. *Biomater Sci*. 2018;6:136–145.
54 Hing KA, Wilson LF, Buckland T. Comparative performance of three ceramic bone graft substitutes. *Spine J*. 2007.
55 Walsh WR, Oliver RA, Christou C, et al. Critical size bone defect healing using collagen-calcium phosphate bone graft materials. *PLoS One*. 2017;12.
56 Grotenhuis N, Bayon Y, Lange JF, Van Osch GJVM, Bastiaansen-Jenniskens YM. A culture model to analyze the acute biomaterial-dependent reaction of human primary macrophages. *Biochem Biophys Res Commun*. 2013;433:115–120.
57 Buttari B, Profumo E, Segoni L, et al. Resveratrol counteracts inflammation in human M1 and M2 macrophages upon challenge with 7-oxo-cholesterol: potential therapeutic implications in atherosclerosis. *Oxid Med Cell Longev*. 2014. https://doi.org/10.1155/2014/257543.
58 Spiller KL, Anfang RR, Spiller KJ, et al. The role of macrophage phenotype in vascularization of tissue engineering scaffolds. *Biomaterials*. 2014. https://doi.org/10.1016/j.biomaterials.2014.02.012.
59 Utomo L, van Osch GJVM, Bayon Y, Verhaar JAN, Bastiaansen-Jenniskens YM. Guiding synovial inflammation by macrophage phenotype modulation: an in vitro study towards a therapy for osteoarthritis. *Osteoarthritis Cartilage*. 2016. https://doi.org/10.1016/j.joca.2016.04.013.
60 Utomo L, Boersema GSA, Bayon Y, Lange JF, Van Osch GJVM, Bastiaansen-Jenniskens YM. In vitro modulation of the behavior of adhering macrophages by medications is biomaterial-dependent. *Biomed Mater*. 2017;12.
61 Tarique AA, Logan J, Thomas E, Holt PG, Sly PD, Fantino E. Phenotypic,functional, and plasticity features of classical and alternatively activated human macrophages. *Am J Respir Cell Mol Biol*. 2015. https://doi.org/10.1165/rcmb.2015-0012OC.
62 Utomo L, Bastiaansen-Jenniskens YM, Verhaar JAN, van Osch GJVM. Cartilage inflammation and degeneration is enhanced by pro-inflammatory (M1) macrophages in vitro, but not inhibited directly by anti-inflammatory (M2) macrophages. *Osteoarthritis Cartilage*. 2016. https://doi.org/10.1016/j.joca.2016.07.018.
63 Barros MHM, Hauck F, Dreyer JH, Kempkes B, Niedobitek G. Macrophage polarisation: an immunohistochemical approach for identifying M1 and M2 macrophages. *PLoS One*. 2013. https://doi.org/10.1371/journal.pone.0080908.
64 Raggi F, Pelassa S, Pierobon D, et al. Regulation of human macrophage M1-M2 polarization balance by hypoxia and the triggering receptor expressed on myeloid cells-1. *Front Immunol*. 2017. https://doi.org/10.3389/fimmu.2017.01097.
65 Xue Q, Yan Y, Zhang R, Xiong H. Regulation of iNOS on immune cells and its role in diseases. *Int J Mol Sci*. 2018. https://doi.org/10.3390/ijms19123805.
66 Gilles Carpentier. Contribution: angiogenesis analyzer. *Imag News*. 2012.
67 Pennings I, van Dijk LA, van Huuksloot J, et al. Effect of donor variation on osteogenesis and vasculogenesis in hydrogel cocultures. *J. Tissue Eng. Regen. Med.* 2019;13:433–445.
68 Croes M, Öner FC, van Neerven D, et al. Proinflammatory T cells and IL-17 stimulate osteoblast differentiation. *Bone*. 2016;84:262–270.
69 Prins HJ, Braat AK, Gawlitta D, et al. In vitro induction of alkaline phosphatase levels predicts in vivo bone forming capacity of human bone marrow stromal cells. *Stem Cell Res*. 2014;12:428–440.
70 Eijken M, Koedam M, Van Driel M, Buurman CJ, Pols HAP, Van Leeuwen JPTM. The essential role of glucocorticoids for proper human osteoblast differentiation and matrix mineralization. *Mol Cell Endocrinol*. 2006, 24887–93.
71 Shihan MH, Novo SG, Le Marchand SJ, Wang Y, Duncan MK. A simple method for quantitating confocal fluorescent images. *Biochem. Biophys. Reports*. 2021;25.
72 Jundt G, Berghäuser KH, Termine JD, Schulz A. Osteonectin - a differentiation marker of bone cells. *Cell Tissue Res*. 1987. https://doi.org/10.1007/BF00218209.
73 Chen W, Zhao Y, Li XC, Kubiak JZ, Ghobrial RM, Kloc M. Rho-specific Guanine nucleotide exchange factors (Rho-GEFs) inhibition affects macrophage phenotype and disrupts Golgi complex. *Int J Biochem Cell Biol*. 2017. https://doi.org/10.1016/j.biocel.2017.10.009.
74 Cui K, Ardell CL, Podolnikova NP, Yakubenko VP. Distinct migratory properties of M1, M2, and resident macrophages are regulated by αdβ2and αmβ2integrin-mediated adhesion. *Front Immunol*. 2018. https://doi.org/10.3389/fimmu.2018.02650.
75 Gao S, Wang Y, Li D, et al. TanshinoneIIA alleviates inflammatory response and directs macrophage polarization in lipopolysaccharide-stimulated RAW264.7 cells. *Inflammation*. 2019. https://doi.org/10.1007/s10753-018-0891-7.
76 Luu TU, Gott SC, Woo BWK, Rao MP, Liu WF. Micro- and nanopatterned topographical cues for regulating macrophage cell shape and phenotype. *ACS Appl Mater Interfaces*. 2015;7:28665–28672.
77 McWhorter FY, Wang T, Nguyen P, Chung T, Liu WF. Modulation of macrophage phenotype by cell shape. *Proc. Natl. Acad. Sci. U.S.A*. 2013. https://doi.org/10.1073/pnas.1308887110.
78 Tylek T, Blum C, Hrynevich A, et al. Precisely defined fiber scaffolds with 40 μm porosity induce elongation driven M2-like polarization of human macrophages. *Biofabrication*. 2020. https://doi.org/10.1088/1758-5090/ab5f4e.
79 Wosik J, Chen W, Qin K, Ghobrial RM, Kubiak JZ, Kloc M. Magnetic field changes macrophage phenotype. *Biophys J*. 2018. https://doi.org/10.1016/j.bpj.2018.03.002.
80 Xiao H, Guo Y, Li B, et al. M2-Like tumor-associated macrophage-targeted codelivery of STAT6 inhibitor and IKKβ siRNA induces M2-to-M1 repolarization for cancer immunotherapy with low immune side effects. *ACS Cent Sci*. 2020. https://doi.org/10.1021/acscentsci.9b01235.
81 Zhu Y, Liang H, Liu X, et al. Regulation of macrophage polarization through surface topography design to facilitate implant-to-bone osteointegration. *Sci Adv*. 2021;7, eabf6654.
82 Lee HH, Tien SC, Jou TS, Chang YC, Jhong JG, Chang ZF. Src-dependent phosphorylation of ROCK participates in regulation of focal adhesion dynamics. *J Cell Sci*. 2010;123:3368–3377.
83 Yang Y, Lin Y, Zhang Z, Xu R, Yu X, Deng F. Micro/nano-net guides M2-pattern macrophage cytoskeleton distribution via Src–ROCK signalling for enhanced angiogenesis. *Biomater Sci*. 2021. https://doi.org/10.1039/d1bm00116g.
84 Haftbaradaran Esfahani P, Knöll R. *Cell Shape: Effects on Gene Expression and Signaling*. Biophys. Rev. Springer; 2020. August 1.
85 McWhorter FY, Davis CT, Liu WF. Physical and mechanical regulation of macrophage phenotype and function. *Cell Mol Life Sci*. 2015. https://doi.org/10.1007/s00018-014-1796-8.
86 Martinez FO, Gordon S. The M1 and M2 paradigm of macrophage activation: time for reassessment. *F1000Prime Rep*. 2014. https://doi.org/10.12703/P6-13.
87 Nahrendorf M, Swirski FK. Abandoning M1/M2 for a network model of macrophage function. *Circ Res*. 2016. https://doi.org/10.1161/CIRCRESAHA.116.309194.
88 Xue J, Schmidt SV, Sander J, et al. Transcriptome-based network analysis reveals a spectrum model of human macrophage activation. *Immunity*. 2014. https://doi.org/10.1016/j.immuni.2014.01.006.
89 Duan R, Zhang Y, van Dijk L, et al. Coupling between macrophage phenotype, angiogenesis and bone formation by calcium phosphates. *Mater Sci Eng C*. 2021;122. Manuscript submitted for publication).
90 Jaquiéry C, Schaeren S, Farhadi J, et al. In vitro osteogenic differentiation and in vivo bone-forming capacity of human isogenic jaw periosteal cells and bone marrow stromal cells. In: *Ann. Surg., 242859–868*. December: Lippincott, Williams, and Wilkins; 2005.
91 Yuan A, Hsiao YJ, Chen HY, et al. Opposite effects of M1 and M2 macrophage subtypes on lung cancer progression. *Sci Rep*. 2015;5.

92 Baer C, Squadrito ML, Iruela-Arispe ML, De Palma M. Reciprocal interactions between endothelial cells and macrophages in angiogenic vascular niches. *Exp Cell Res*. 2013. https://doi.org/10.1016/j.yexcr.2013.03.026.

93 Du Cheyne C, Tay H, De Spiegelaere W. The complex TIE between macrophages and angiogenesis. *J Vet Med Ser C Anat Histol Embryol*. 2020. https://doi.org/10.1111/ahe.12518.

94 Zhang Y, Böse T, Unger RE, Jansen JA, Kirkpatrick CJ, van den Beucken JJJP. Macrophage type modulates osteogenic differentiation of adipose tissue MSCs. *Cell Tissue Res*. 2017. https://doi.org/10.1007/s00441-017-2598-8.

95 Chambers SEJ, O'Neill CL, Guduric-Fuchs J, et al. The vasoreparative function of myeloid angiogenic cells is impaired in diabetes through the induction of IL1β. *Stem Cell*. 2018. https://doi.org/10.1002/stem.2810.

96 Jetten N, Verbruggen S, Gijbels MJ, Post MJ, De Winther MPJ, Donners MMPC. Anti-inflammatory M2, but not pro-inflammatory M1 macrophages promote angiogenesis in vivo. *Angiogenesis*. 2014. https://doi.org/10.1007/s10456-013-9381-6.

97 Sun M, Qiu S, Xiao Q, et al. Synergistic effects of multiple myeloma cells and tumor-associated macrophages on vascular endothelial cells in vitro. *Med Oncol*. 2020;37:99.

98 Wang J, Qian S, Liu X, et al. M2 macrophages contribute to osteogenesis and angiogenesis on nanotubular TiO2 surfaces. *J Mater Chem B*. 2017;5:3364–3376.

99 Xu WC, Dong X, Ding JL, et al. Nanotubular TiO 2 regulates macrophage M2 polarization and increases macrophage secretion of vegf to accelerate endothelialization via the ERK1/2 and PI3K/AKT pathways. *Int J Nanomed*. 2019;14:441–455.

100 Xiao D, Zhang J, Zhang C, et al. The role of calcium phosphate surface structure in osteogenesis and the mechanisms involved. *Acta Biomater*. 2020. Acta Materialia Inc, April 1.

101 Dos Santos EA, Farina M, Soares GA, Anselme K. Surface energy of hydroxyapatite and β-tricalcium phosphate ceramics driving serum protein adsorption and osteoblast adhesion. *J Mater Sci Mater Med*. 2008;19:2307–2316.

102 Davison NL, Su J, Yuan H, van den Beucken JJJP, de Bruijn JD, de Groot FB. Influence of surface microstructure and chemistry on osteoinduction and osteoclastogenesis by biphasic calcium phosphate discs. *Eur Cell Mater*. 2015;29:314–329.

103 Engel E, Del Valle S, Aparicio C, et al. Discerning the role of topography and ion exchange in cell response of bioactive tissue engineering scaffolds. *Tissue Eng*. 2008;14:1341–1351.

104 Dos Santos EA, Farina M, Soares GA, Anselme K. Chemical and topographical influence of hydroxyapatite and β-tricalcium phosphate surfaces on human osteoblastic cell behavior. *J Biomed Mater Res, Part A*. 2009;89:510–520.

105 Anderson JA, Lamichhane S, Mani G. Macrophage responses to 316L stainless steel and cobalt chromium alloys with different surface topographies. *J Biomed Mater Res, Part A*. 2016;104:2658–2672.

106 Hotchkiss KM, Reddy GB, Hyzy SL, Schwartz Z, Boyan BD, Olivares-Navarrete R. Titanium surface characteristics, including topography and wettability, alter macrophage activation. *Acta Biomater*. 2016;31:425–434.

107 Lamichhane S, Anderson JA, Vierhout T, Remund T, Sun H, Kelly P. Polytetrafluoroethylene topographies determine the adhesion, activation, and foreign body giant cell formation of macrophages. *J Biomed Mater Res, Part A*. 2017;105:2441–2450.